1 November 2001

ELSEVIER

Optics Communications 198 (2001) 293–309

OPTICS COMMUNICATIONS

www.elsevier.com/locate/optcom

Interferometric characterization of spatial coherence of high energy synchrotron X-rays

V. Kohn [a], I. Snigireva [b], A. Snigirev [b,*]

[a] *Russian Research Centre, "Kurchatov Institute", 123182 Moscow, Russia*
[b] *European Synchrotron Radiation Facility, BP220, F-38043 Grenoble, France*

Received 30 March 2001; received in revised form 27 June 2001; accepted 5 September 2001

Abstract

A simple and direct interferometric technique for characterization of the source size and the transverse coherence length of synchrotron hard X-rays is discussed. A high level of spatial coherence of the X-ray beam allows us to detect the diffraction images (phase contrast patterns) of both the boron fiber of about 100 μm diameter and the slit of different widths. We characterize the level of coherence by comparison of the measured visibility of the interference fringes with the theoretical values by means of simple analytical formulas derived in this work. The analytical theory of both the fiber and the slit diffraction images is discussed in details. The results obtained analytically are confirmed by computer simulations. The proposed technique is well suited for third-generation synchrotron sources and was applied at the European Synchrotron Radiation Facility.

Keywords: Spatial coherence; Hard X-rays; Synchrotron radiation; Slit interference pattern; Fiber interference pattern; Visibility

1. Introduction

With an advent of third-generation synchrotron radiation sources such as ESRF, SPRing-8 and APS coherent optics has been extended to the field of hard X-ray radiation. The high spatial coherence, the really unique feature of these new sources, results from a very small source size of about 30 μm and large source-to-object distance (around 50–100 m). Using such a laser-like beam, coherent imaging techniques such as phase contrast imaging, holography and interferometry have been proposed [1–7] and are currently under intensive development [8–11]. State of the art on-line detectors [12], together with optical elements created on diffraction and refraction principles [13–18], open real opportunities to overcome visible light limits and to go to submicrometer and even to nanometer resolution. Under these new conditions the characterization and the manipulation of coherence are of great importance.

Generally associating coherence with the ability to observe interference phenomena, we should distinguish between temporal coherence linked to the spectral bandwidth (monochromaticity) of the beam and spatial (transverse) coherence which is related to the source size. In the soft X-ray domain interferometry techniques were used for coherence measurement [19–21]. To define the coherence in the field of hard X-rays, optical elements such as

* Corresponding author. Fax: +33-4-76-88-25-42.
E-mail address: snigirev@esrf.fr (A. Snigirev).

0030-4018/01/$ - see front matter
PII: S0030-4018(01)01544-9

crystals [22] and mirrors [23] were applied. However, as has been demonstrated [24–27] the mirrors may introduce additional distortions in the interference pattern. In particular, as it was pointed out, X-ray beam heterogeneity in cross-section owing to surface roughness of beryllium windows were observed [28]. The problem can be solved by proper polishing beryllium windows. The coherence measurement based on the Talbot effect was also performed [29] using a phase grating. The method demands a measurement of periodical intensity distribution at different distances behind the object.

In this work we discuss in detail a simple and direct interferometric technique for a characterization of spatial coherence of synchrotron X-ray beams. Preliminary results were reported in Ref. [30]. The technique consists of measuring the visibility of interference fringes observed on the diffraction image of round transparent fiber as well as on the central or edge diffraction images of the slit of different sizes. The incident radiation is only partially coherent, i.e., the transverse coherence length at the object is not infinite. In other words, coherent images are partially destroyed by averaging over the source size. To determine the source size and the transverse coherence length one may compare the visibility of the fringes with the "ideal" visibility for a point source. The latter must be calculated theoretically. Such a method was used as early as in 1957 in Ref. [31]. We developed the analytical theory of diffraction images for both the fiber and the slit. The theory allows us to derive the simple formulas for the ideal visibility, for the source size and for the transverse coherence length. To examine this approach we have performed the experimental study of the interference patterns produced by boron fiber of 100 μm diameter and slits of different sizes.

The experimental results are presented in Section 2. We have obtained the vertical transverse source size as (33 ± 4) μm from the fiber and (35 ± 3) μm from the slit of 100 μm width. The results coincide very closely and are in accordance with the data provided by the ESRF machine group at the time of the experiment. The general theory of the interference pattern formation with the partially spatial coherent X-ray beams is reviewed in Section 3. We discuss the approach based on the mutual coherence function. However, considering the simple in-line holography setup, it is more convenient to analyze the diffraction pattern with perfectly coherent beam and then to average the fringe pattern over the region of source size projected to the detector.

The analytical theory of the fringe pattern formation in the part outside the fiber shadow is presented in the Section 4. An usage of both the geometrical optics approach and the stationary phase method are analyzed in details. As is known in this region the fringes are formed due to the interference of two groups of rays. One of them reaches the detector directly passing through the air while another one is deviated by the fiber edge. To derive a more accurate approximation we develop the enhanced stationary phase technique. The analytical theory of the slit diffraction pattern is presented in Section 5. In general the interference fringes are described by Fresnel integrals. Under some conditions the asymptotic behavior of the Fresnel integrals can be used that simplifies the analysis. Both the Fresnel central fringe of the relatively narrow slit and the edge fringes of the wide slit are analyzed and the formulas for the evaluation of the source size and transverse coherence length are derived.

2. Experimental results

The experiments were performed with the in-line holography experimental setup at the undulator beamline ID22 of the European Synchrotron Radiation Facility (ESRF, Grenoble). This beamline is well adapted for microimaging experiments with coherent X-rays due to the small source size, low divergence and high intensity (up to 10^{13} photons/mm^2) at the sample position. The interference fringes of well calibrated microobjects, namely, the fiber and the slit were studied. The energy of X-rays was selected by a silicon single crystal (1 1 1) monochromator in the range of 10–20 keV. We assume that the monochromator is perfect, and it does not influence spatial coherence of the beam. On the other hand, using the monochromator based on Bragg diffraction we

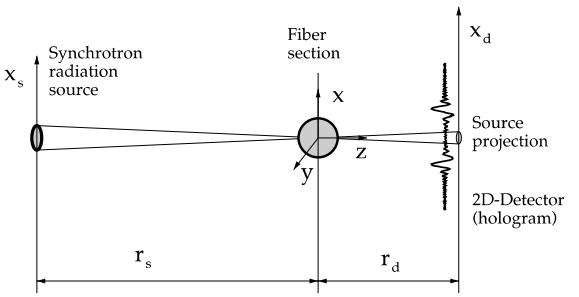

Fig. 1. The scheme of experimental setup for a study of X-ray diffraction on a fiber.

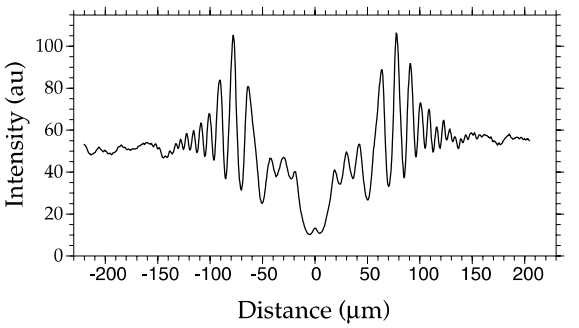

Fig. 2. Diffraction image of 100 μm diameter boron fiber with 15 μm tungsten core recorded at the distance $r_d = 5$ m with 17 keV X-rays and source-to-fiber distance $r_s = 41$ m.

may consider the radiation as completely monochromatic. Therefore we exclude below the monochromator from an analysis.

The experimental configuration is simple and straightforward. It is assumed that the microobject like a fiber is illuminated by approximately spherical coherent wave. The detector registers both a primary radiation and a radiation scattered by microobject (see Fig. 1). Contrary to laser optics [32], in a high energy X-ray domain a small object of few ten microns diameter is completely or partially transparent. Therefore it produces, mainly, a phase shift of the incident wave. The fiber was located at the long distance r_s from the source. The interference patterns were collected using a 1 μm thick transparent YAG scintillator coupled by a light microscope to a CCD camera. The detector has a pixel size of 0.32 μm and the FWHM of the point-spread function is approximately 0.8 μm [12]. The detector was placed at the distance r_d from the object. The interference between the direct rays and the rays scattered by microobject results in the intensity oscillations of varying amplitudes and periodicity (see Fig. 1).

Fig. 2 shows the intensity distribution at the detector (in-line hologram) for the boron fiber of 50 μm radius having a tungsten core of 7.5 μm radius measured under the following experimental conditions: $r_s = 41$ m, $r_d = 5$ m. The monochromator was used to select the energy of X-rays $\hbar\omega = 17$ keV. One may see a series of well pronounced fringes on the in-line hologram in the part outside the fiber shadow. However, the fringes are observed with an uneven background. This is due to extra perturbations of the initial wave front of the beam by some optical elements installed on the X-ray beam path, for example, a beryllium window. The problem of eliminating such a perturbation may be formulated as a problem of coherence preservation. The X-ray beam stays coherent, but it has undesirable perturbation of the wave front. However, in experiments we need a beam with the known properties like a spherical wave. Therefore the only optical elements may be used which do not disturb the phase profile of the coherent wave. It is more strong requirement than a simple prevention of intensity loss.

We have measured the visibility of different unperturbed fringes. The variable visibility $V(x)$ is introduced similarly to the definition of Michelson [33]. However, it shows the visibility of fringe located at the point x, namely

$$V(x) = \frac{I(x)_{\max} - I(x)_{\min}}{I(x)_{\max} + I(x)_{\min}} \tag{1}$$

where $I(x)_{\max}$ and $I(x)_{\min}$ are the maximum and adjusted minimum values of intensity at the point x. The visibility of several fringes were used to calculate the source size as $w_s = (33 \pm 4)$ μm and the transverse coherence length as $l_{tc} = \sqrt{2}\lambda r_s/\pi w_s = (41 \pm 5)$ μm by means of the analytical formulas derived theoretically in this work (see below).

Similar experimental setup was used to study X-ray diffraction by a slit (see Fig. 3). Such an experiment is well known in the visible light domain. However, up to now it was very difficult for hard X-rays. As known, if a width a of the slit is

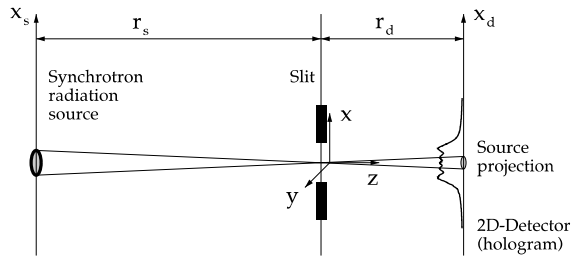

Fig. 3. The scheme of experimental setup for a study of X-ray diffraction on a slit.

much larger than a wavelength λ, then at short distances the slit restricts only the beam size without a change of intensity. In the narrow region near the slit edges the fringes of Fresnel diffraction at the edges are observed with variable a distance between them and a visibility. With increasing the distance r_d the Fresnel diffraction occurs when the interference fringes inside the slit shadow are observed. At longer distances $r_d \gg a^2/\lambda$ the Fraunhofer diffraction takes place.

The measurements of diffraction images of the slit were done with the slightly different distances $r_s = 31$ m, $r_d = 10$ m and with X-ray energy $\hbar\omega = 18$ keV. Fig. 4 shows the intensity profiles obtained for slits of different widths. One may see the transition from Fraunhofer to Fresnel diffrac-

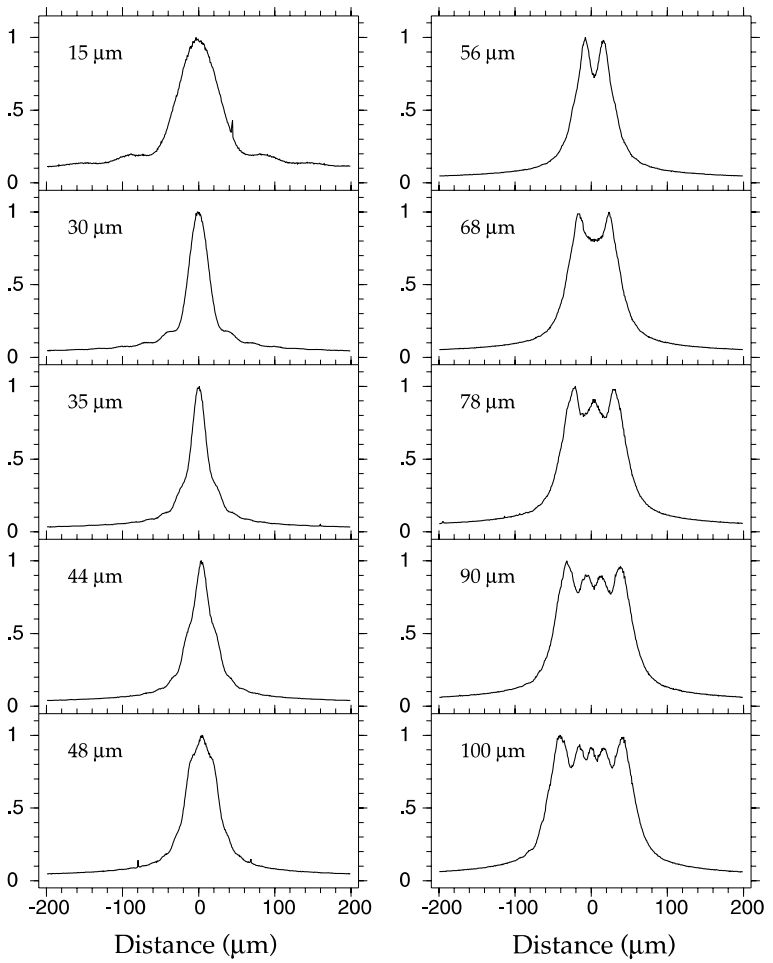

Fig. 4. Diffraction images of slits of different sizes pointed at the plots recorded at the distance $r_d = 10$ m with 18 keV X-rays and source-to-fiber distance $r_s = 31$ m.

tion with increasing the slit size. In the first case the width of the slit image has a reverse dependence on the slit size. In the second case there is a correspondence between the slit width and the image width and the interference fringes appear inside the region of slit shadow. It is easy to measure the visibility of the central fringe of the 100 μm slit image as $V = 0.11 \pm 0.01$. Then using the theoretical formulas derived in this work (see below) we estimate the source size as $w_s = (35 \pm 3)$ μm and the transverse coherence length as $l_{tc} = (27 \pm 2)$ μm. The transverse coherence length is smaller in this case due to the smaller value of the source-to-slit distance. We note that the effective source size is in accordance with the data provided by ESRF machine group at the time of experiment.

3. General theory

3.1. Definition of the problem

As is known, the monochromatic wave of a point source is entirely coherent. In reality, the synchrotron radiation source consists of very many incoherent point sources transversely distributed according to the Gaussian law. Each point source radiates an approximately spherical wave of finite bandwidth. It is usual practice to distinguish between the temporal coherence and the spatial coherence [34] which describe the time and space properties of the scattering process. The temporal coherence relates directly to the effective bandwidth of the radiation used in the experiment. On the other hand, it is connected with the finite duration of individual X-ray flashes, the so-called coherence time t_c. This value determines the coherence length of a wave train $l_c = ct_c$, where c is a speed of light. In the high energy X-ray domain it is more convenient to measure temporal coherence directly by the bandwidth $\Delta\omega = 2\pi/t_c$. As is shown [35], one may take into account the temporal coherence in a calculation considering the scattering processes for the monochromatic radiation of frequency ω and then averaging the intensity over the effective bandwidth $\Delta\omega$, because very many wave trains with different initial phases go from the source to the detector during the experiment.

Spatial coherence is related mainly to the source size. The radiation from different points of the source is incoherent due to the absence of the phase correlation between the different flashes since individual X-ray radiators are the internal electrons of atoms or the electrons in a storage ring. In the case of extended source interference fringes from the point source can be resolved if they are not spoiled by the source size. For in-line geometry only the source projection is important, as shown in Figs. 1 and 3. On the other hand, the fact of contrast degradation up to complete disappearance of the fringes may be used for a characterization of spatial coherence.

Considering the spatial coherence in this work we shall assume a monochromatic radiation and restrict ourselves to objects having a homogeneous structure in one direction like the fiber and the slit. Such a direction is connected with y-axis. Let us begin with the point radiator located at the coordinate x_s on the source. The Fresnel–Kirchhoff formula [36] allows us to write a ratio of the wavefield strength $E(x_d)$ of the wave scattered by object and the wavefield strength $E_S(x_d)$ in the case without the object as follows:

$$\frac{E(x_d)}{E_S(x_d)} = P^{-1}(x_d - x_s, r_t) \int_{-\infty}^{\infty} dx P(x_d - x, r_d) \times F_o(x) P(x - x_s, r_s) \tag{2}$$

where x_d is the coordinate at the detector, r_s is a distance from the source to the object, r_d is a distance from the object to the detector (see Figs. 1 and 3), $r_t = r_s + r_d$, $P(x, r)$ is the propagator of the transverse part of the wavefield along x-direction

$$P(x, r) = \frac{1}{\sqrt{i\lambda r}} \exp\left(i\pi \frac{x^2}{\lambda r}\right) \tag{3}$$

Here λ is a wavelength of the radiation. Only x-component of the wavefield is disturbed by the transmission function $F_o(x)$ of the object.

In general case the transmission function $F_o(x)$ is a complex value. When the fiber of tens micron radius R is of interest, we can neglect a deviation of rays inside the object and use $F_o(x)$ as unity for $x^2 > R^2$ and

$$F_o(x) = \exp[i\varphi(x)] = \exp\left(-\frac{4\pi}{\lambda}(i\delta+\beta)\sqrt{R^2-x^2}\right),\ x^2 < R^2 \tag{4}$$

Here δ and β are defined by the relation $n = 1-\delta+i\beta$ where n is the complex index of refraction and δ and β are called the refractive index decrement and absorption index respectively [37]. When the object contains several fibers the sum of the expressions (4) has to be considered. The fiber used in the experiment has a tungsten core. In the accurate calculations the core was taken into account. However, an analytical approximation it derived for the fiber without a core. In the case of the slit of width a the transmission function $F_o(x)$ has an evident form

$$F_o(x) = \begin{cases} 0, & |x| > a/2 \\ 1, & |x| < a/2 \end{cases} \tag{5}$$

Substituting Eq. (3) to Eq. (2) we may transform the expression to the next form

$$\frac{E(x_d)}{E_S(x_d)} = \frac{1}{\sqrt{i\lambda r_r}}\int_{-\infty}^{\infty} dx \exp\left(i\frac{\pi}{\lambda r_r}\left[x - x_{ds}\frac{r_s}{r_t}\right]^2\right)F_o(x) \tag{6}$$

where $r_r = r_s r_d/r_t$ is a reduced object-to-detector distance, $x_{ds} = x_d + x_s r_d/r_s$. This expression contains only the reduced coordinate x_{ds} instead of x_d and x_s separately. Therefore it is sufficient to calculate the diffraction image (intensity) of the object for a spherical wave originating from the central point of the source and then to make an average value of the intensity over the projection of the transverse source size to the detector plane because different points on the source are incoherent. Below, calculating the intensity for the point source we use x_d instead of x_{ds}.

Let the brightness distribution $B(x_s)$ inside the source be a Gaussian with a width w_s and $\rho_s = w_s/2$, namely

$$B(x_s) = \frac{1}{\rho_s\sqrt{\pi}}\exp\left(-\frac{x_s^2}{\rho_s^2}\right) \tag{7}$$

The normalized intensity of interference fringes $I(x_d)$ corresponding the experimental value must be calculated as a convolution of an ideal fringe pattern $I_0(x_d)$ (for a point source) with the source brightness distribution taking into account the magnification factor r_d/r_s as follows:

$$I(x_d) = \int_{-\infty}^{\infty} dx_s B(x_s) I_0\left(x_d + x_s\frac{r_d}{r_s}\right) \tag{8}$$

The formulas presented above allows one to calculate numerically accurate diffraction images of the fiber and the slit. Then the visibility $V(x_d)$ may be calculated using Eq. (1).

3.2. Mutual coherence function

The approach presented above takes into account the partial spatial coherence due to the finite source size by integrating over a source size directly. There is another approach which deals with the mutual coherence function [33] (see also Ref. [38]). The expression for the normalized intensity can be written from Eq. (6) as follows:

$$I_0(x_d) = \int dx\,dx' \frac{F_o(x)F_o^*(x')}{\lambda r_r} \times \exp\left(\frac{i\pi}{\lambda r_r}\left[x^2 - x'^2 - 2(x-x')x_d\frac{r_s}{r_t}\right]\right) \tag{9}$$

This expression contains the intensity at the detector point x_d as a result of a correlation between two different points x and x' on the object.

Since the detector records the intensity from all point radiators of the source simultaneously, we have to use Eq. (8) once again. The result may be written as

$$I(x_d) = \int dx\,dx' F_o(x)F_o^*(x')\mu(x-x')\frac{1}{\lambda r_r} \times \exp\left(\frac{i\pi}{\lambda r_r}\left[x^2 - x'^2 - 2(x-x')x_d\frac{r_s}{r_t}\right]\right) \tag{10}$$

The difference between the expressions of Eqs. (9) and (10) consists of the appearance of the function $\mu(x)$ that describes the mutual coherence of two points at the object having the distance x between them. It is determined as follows:

$$\mu(x) = \frac{1}{\rho_s\sqrt{\pi}} \int_{-\infty}^{\infty} dx_s \exp\left(-\frac{2\pi i}{\lambda r_s} x x_s - \frac{x_s^2}{\rho_s^2} \right) = \exp\left(-\frac{x^2}{2l_{tc}^2} \right) \quad (11)$$

where

$$l_{tc} = \frac{\sqrt{2}\lambda r_s}{\pi w_s} \quad (12)$$

is the transverse coherence length. It follows from Eq. (11) that the correlation between the points x and x' is high enough, i.e., $\mu(x) \approx 1$, for very small source size w_s or for very large source-to-object distance r_s.

Unfortunately the theory does not give the way of calculating the parameter l_{tc} directly from the experimental interference fringes for rather complicated objects. The exception is only two narrow slits separated by the distance l when the transmission function may be approximated by sum of two delta functions $F_o(x) = \delta(x - l/2) + \delta(x + l/2)$. No other way except fitting the formulas (10) and (11) is seen. However, fitting the experimental data using the formulas (10) and (11) is more complicated than a usage of the direct formulas (6)–(8). Besides, Eq. (8) gives an understanding that the apparent decrease of the visibility of fringes has to occur when the distance between the registered fringes d_f is smaller than the projection of the source size, namely, $d_f < w_s r_d / r_s$.

4. Analytical theory of the fiber image

4.1. Geometrical optics

The experimental diffraction pattern of the round fiber (see Fig. 2) shows a series of well resolved interference fringes in the part outside the fiber shadow. This fact reveals, on the one hand, that the synchrotron radiation beam is spatially coherent. On the other hand, it opens a possibility to measure the source size from the visibility of the fringes. However, this technique becomes quantitatively effective if the theory proposing some simple relation between the parameters of experimental setup, the visibility of the fringes and the source size is developed. It is evident that the fringes outside the fiber shadow arise owing to the interference between two groups of rays. The rays of the first group go directly from the source to the detector. The rays of the second group fall on the fiber edge, deviate at the air–fiber interfaces due to refraction, and arrive finally to the same place at the detector, as it is shown in Fig. 5.

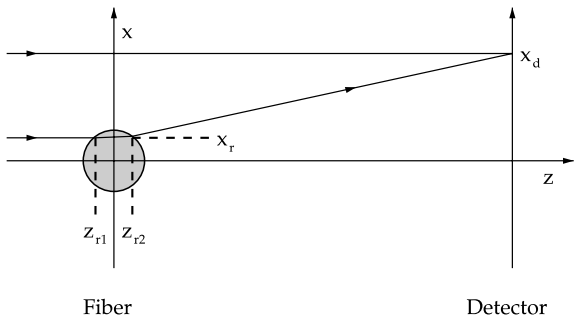

Fig. 5. The trajectories of interfering rays. The bottom ray is deviated due to a refraction on the fiber boundaries according to Snell's law.

As is known, the interference phenomena are observed with a coherent radiation characterized by the well determined wavelength λ and the direction of propagation [33]. The interference maxima appear as a result of optical path difference of integer number of wavelengths between the interfering waves. In a simple case of two plane waves this difference arises when the waves intersect each other in space at the definite angle $\Delta\theta$. The ray path difference $\Delta r_{12} = \Delta x \Delta\theta$ where Δx is the distance between two points on the fringe pattern. Therefore the distance between two neighboring strips (the period of intensity oscillations) equals $\Delta x = \lambda/\Delta\theta$. If the angle $\Delta\theta$ is very small, the fringes can be directly recorded even for hard X-rays.

In the case of fiber the angle $\Delta\theta$ between intersecting rays is not constant in space. It increases continuously with increasing the distance from the edge of the fiber shadow at the image plane. As a result, the distance between neighboring fringes decreases. Hence we obtain the ruler with a variable scale which allows us to measure a source size. To explain physical nature of the phenomenon we consider here the approximation of geometrical optics.

It is assumed in the geometrical optics that the incident radiation may be represented by the set of rays each of them corresponds to a small part of the wave front. Each ray moves in accord with the local optical conditions and undergoes a reflection or a refraction at the interfaces between two media having different optical densities. Each ray may be characterized by the coordinate in the plane normal to its direction of propagation. We are considering the in-line geometry with the z-axis as the optical axis, y-axis as a fiber axis and x-axis as an axis of fiber imaging (see Fig. 1). The distance between the point source and the fiber is r_s, the fiber-to-detector distance is r_d. We restrict ourselves by the case when $r_s \gg r_d$ that allows us to neglect the initial divergence of the rays compared to the deviations produced by fiber.

We place the origin of the coordinate system at the center of the fiber (see Fig. 1). Therefore the section of the fiber surface is described by the equation $x^2 + z^2 = R^2$ where R is the fiber radius. All incoming rays are parallel to the z-axis and are characterized by the coordinate x_r (see Fig. 5). When $0 < x_r < R$ the ray falls on the fiber at the point $z_{r1} = -(R^2 - x_r^2)^{1/2}$. It is easy to calculate the small change in the direction of the ray at the air–fiber interface using the Snell's law in a linear approximation. The angle between z-axis and the ray changes its value from zero to $\varphi_1 = \delta x_r (R^2 - x_r^2)^{-1/2}$ where δ is a decrement of refractive index. The value of δ is usually less than 10^{-6} for hard X-rays. Therefore we neglect the change of x-coordinate inside the fiber. The ray leaves the fiber–air interface at $z_{r2} = (R^2 - x_r^2)^{1/2}$. Therefore the angle of deviation from the z-axis will be increase once again by the same value and becomes $\varphi_2 = 2\varphi_1$.

In the air the ray reaches the detector at the point

$$x_d = x_r + \varphi_2 r_d = x_r \left(1 + \frac{\tilde{a}}{(R^2 - x_r^2)^{1/2}} \right) \tag{13}$$

where $\tilde{a} = 2\delta r_d$. For the estimation we will consider the parameters of the experiment: the energy of X-rays $E = 17$ keV and the distance $r_d = 5$ m. In this case $\delta = 1.55 \times 10^{-6}$ and $\tilde{a} = 2\delta r_d = 15.5$ μm. Hence the considerable deviation of the ray trajectory may occur only for ray that has an initial coordinate near the fiber edge when the difference $(R - x_r)$ is small. For these rays we calculate the approximate reverse dependence

$$x_r \approx R \left(1 - \frac{\tilde{a}^2}{2(x_d - R)^2} \right) \tag{14}$$

The intensity of radiation is characterized by the density of rays. The initial density is constant dx_r. The density of rays scattered by the fiber is not constant

$$\begin{aligned} dx_d &= \left(1 + \frac{\tilde{a} R^2}{\left(R^2 - x_r^2\right)^{3/2}} \right) dx_r \\ &= \left(1 + \frac{(x_d - R)^3}{\tilde{a}^2 R} \right) dx_r \end{aligned} \tag{15}$$

The total wavefield for $x_d > R$ will be a sum of two contributions from a direct ray and the ray deviated by the fiber. The phase difference between these two rays is defined by their optical path difference. It can be calculated approximately under the same conditions as follows:

$$\Delta\psi(x_d) = \frac{\pi}{\lambda r_d} \left[(x_d - R)^2 - \frac{2\tilde{a}^2 R}{(x_d - R)} \right] \tag{16}$$

Now the expression for the normalized intensity which describes the fringe pattern looks as

$$I_0(x_d) = 1 + \tilde{A}^2(x_d) + 2\tilde{A}(x_d) \cos[\Delta\psi(x_d)] \tag{17}$$

where $\tilde{A}(x_d) = (dx_r/dx_d)^{1/2}$. This expression describes the fringes having increasing a local density and decreasing a local contrast with increasing the distance from the fiber edge $(x_d - R)$. The distance between neighboring strips can be estimated as

$$\begin{aligned} \Delta x_d &= \frac{2\pi}{d\Delta\psi/dx_d} = \frac{\lambda r_d}{(x_d - R)\left(1 + \tilde{f}(x_d)\right)^{1/2}}, \\ \tilde{f}(x_d) &= \frac{\tilde{a}^2 R}{(x_d - R)^3} \end{aligned} \tag{18}$$

We note the expression is just the λ/φ_2 within the accepted approximation. The function $\tilde{f}(x_d)$ describes the phase difference due to the path of the

ray inside the fiber having non-zero decrement of refractive index. An estimation of $\tilde{f}$ in the point $x_d = 2R$ for the parameters of experiment is $(\tilde{a}/R)^2 = 0.096$. This small value allows us to conclude that the distance between far fringes is, mainly, the reciprocal of the distance from the fiber edge.

The function $\tilde{A}(x_d)$ characterizes the variable amplitude of intensity oscillations. For the considered region of the fiber image it can be expressed through the same function $\tilde{f}(x_d)$ as

$$\tilde{A}(x_d) = \frac{\tilde{f}^{1/2}(x_d)}{[1+\tilde{f}(x_d)]^{1/2}} \tag{19}$$

It depends on the distance from the fiber edge approximately as $(x_d - R)^{-3/2}$ for far fringes.

4.2. Stationary phase method

The approximation of geometrical optics is valid for short distances from the known phase front, for hard radiation, and when the perturbed phase front is a slowly varying function in space. In other words, the size of significant region of perturbation of the wave front Δx must be much larger than the radius of the first Fresnel zone $(\lambda r_d)^{1/2}$. However, in our case this condition is not fulfilled in the region near the fiber edge because a jump of the phase shift is significant, and the phase profile has the infinite second derivative. Therefore the formulas obtained above will give an apparent difference for far fringes from the fiber shadow as compared to the results of accurate calculations by means of Fresnel–Kirchhoff formula (2). In this section we obtain the enhanced analytical approximation.

We note that the formulas obtained above by method of geometrical optics (ray tracing) can be derived from the accurate integral of Eq. (6) applying the stationary phase method. First of all, we write the integral (6) for $x_s = 0$, in the form more convenient for a computer simulation

$$\frac{E(x_d)}{E_S(x_d)} = 1 + \frac{1}{\sqrt{i\lambda r_r}} \int_{-R}^{R} dx(\exp[i\varphi(x)] - 1) \times \exp\left(i\frac{\pi}{\lambda r_r}\left[x - x_d\frac{r_s}{r_t}\right]^2\right) \tag{20}$$

Here the phase $\varphi(x)$ is defined by Eq. (4). Below we assume the fiber to be transparent and we neglect β. The stationary phase method [39] consists of using the following relation:

$$\int dx \exp[i\phi(x)] \approx \sum_{k=1}^{n}\left[\frac{2\pi i}{\phi''(x_k)}\right]^{1/2} \exp[i\phi(x_k)] \tag{21}$$

where a summation is performed over all roots of the equation $\phi'(x_k) = 0$, n is a number of the roots. Here $\phi' = d\phi/dx$, $\phi'' = d^2\phi/dx^2$.

In our case the integral in Eq. (20) is taken in the limited region. Therefore we need to assume that the integral is equal to zero if the point of the stationary phase x_k lies out of the region of integrating. It is easy to calculate that the second term in Eq. (20) without the factor $\exp[i\varphi(x)]$ has only one stationary point $x_2 = x_d r_s/r_t$. In the region of our interest where $x_d > Rr_t/r_s$ this term does not contribute. The first term has also only one stationary point x_1 that is a root of the following equation:

$$\phi'(x_1) = \frac{2\pi}{\lambda r_r}\left[x_1\left(1 + \frac{a}{(R^2 - x_1^2)^{1/2}}\right) - x_2\right] = 0 \tag{22}$$

where $a = 2\delta r_r$. At this point the phase value is equal to

$$\phi(x_1) = \frac{\pi}{\lambda r_r}\left[(x_2 - x_1)^2 - \frac{2a^2 x_1}{(x_2 - x_1)}\right] \tag{23}$$

and the second derivative of the phase is equal to

$$\phi''(x_1) = \frac{2\pi}{\lambda r_r}\left[1 - \frac{R^2}{a^2}\left(1 - \frac{x_2}{x_1}\right)^3\right] \tag{24}$$

Finally, applying the approximation of Eq. (21) to the integral of Eq. (20) we obtain the next expression for the intensity distribution at the detector

$$I_0(x_d) = 1 + A^2(x_d) + 2A(x_d)\cos[\phi(x_d)] \tag{25}$$

where $\phi(x_d)$ is defined by Eq. (23) assuming that x_d is an argument, while the coordinates x_1 and x_2 depend on x_d. The function $A(x_d)$ is equal to

$$A(x_d) = \frac{f^{1/2}(x_d)}{[1+f(x_d)]^{1/2}},$$
$$f(x_d) = \frac{a^2 x_1^3}{R^2(x_2 - x_1)^3} \tag{26}$$

We note that the formulas (23)–(26) coincide with the formulas (16)–(19) if x_2, x_1 and a are replaced correspondingly by x_d, R and $\tilde{a}$. Such a replacement is valid approximately when $r_s \gg r_d$ and $x_d \gg 2R$. The formulas obtained in this section are more accurate but more complicated. Fortunately, the replacement of x_1 by R is well enough for far fringes counted from the fiber shadow. However, if the ratio r_d/r_s is not very small then the usage of the parameter x_2 instead of x_d is necessary.

Thus, we find that the result obtained within the geometrical optics is equivalent to the approximation (21). However, this approximation is valid for the integral having rather wide limits of integration when the point of stationary phase is not close to the limits. In our case such a condition is not fulfilled for fringes located at large distance from the fiber shadow when $(x_d - R) \gg R$ and $(R - x_1) \ll R$. We want to propose the enhanced approximation of the stationary phase method based on the following idea. In the standard stationary phase approach one takes into account the Taylor expansion of the phase up to the quadratic term and then replace the limits of integrating by infinity. We may keep the real limit of the integral. In this case the formula (21) is transformed to

$$\int_{-R}^{R} \mathrm{d}x \exp[\mathrm{i}\phi(x)] \approx \left[\frac{2\pi\mathrm{i}}{\phi''(x_1)}\right]^{1/2} \exp[\mathrm{i}\phi(x_1)] \times G(x_t - x_1, x_1 - x_b, \phi''(x_1)) \tag{27}$$

where x_1 is a root of Eq. (22), as before, and the complex function $G(a,b,c)$ is defined by

$$G(a,b,c) = \left[F\left(a(c/\pi)^{1/2}\right) + F\left(b(c/\pi)^{1/2}\right)\right] \tag{28}$$

Here $F(x)$ is a complex normalized Fresnel integral

$$F(x) = \frac{1}{\sqrt{2\mathrm{i}}} \int_0^x \mathrm{d}t \exp\left(\mathrm{i}\frac{\pi}{2}t^2\right) \tag{29}$$

The parameters x_b and x_t have a meaning of new limits of integration. They should be determined from the condition that the approximate expression for the phase $\tilde{\phi}(x) = \phi(x_1) + \phi''(x_1)(x - x_1)^2/2$ at these limits gives the same value of the phase as the real expression gives at the real limits, namely, $\phi(R) = \tilde{\phi}(x_t)$, $\phi(-R) = \tilde{\phi}(x_b)$. This is necessary to conserve the total number of oscillations. For example, $(x_t - x_1)^2 = 2[\phi(R) - \phi(x_1)]/\phi''(x_1)$, and similar relation may be obtained for x_b. As a result we arrive at the enhanced value of the function $A(x_d)$ as follows:

$$A(x_d) = \frac{g(x_d) f^{1/2}(x_d)}{[1+f(x_d)]^{1/2}} \tag{30}$$

where $g(x_d)$ is a modulus of the complex function $G(x_t - x_1, x_1 - x_b, \phi''(x_1))$.

We note that the function $F(x)$ has small values for small arguments, and it equals 1/2 for large arguments. Therefore the function $g(x_d) \approx 0.5$ for far fringes counted from the fiber shadow when $(x_d - R) \gg R$ and x_1 is close to R. Only considering the fringes located near the fiber shadow we may neglect the correcting function $g(x_d)$ and use the standard stationary phase technique (and ray tracing) when $g(x_d) = 1$. Of course, in the region $x_d < -Rr_t/r_s$ the picture is symmetrical.

4.3. Visibility and a source size measurement

To measure the source size we consider the part of fringe pattern where the size of the source projection is less than the distance between the fringes. Under this condition we may treat a slowly varying amplitude of intensity beats as constant. When averaging the cosine function we take only the first (main) term in the phase (23) and replace x_1 by R. As a result, we arrive at the following expression for the integral of Eq. (8):

$$I(x_d) = 1 + A^2(x_d) + 2A(x_d)C(x_d) \tag{31}$$

where

$$C(x_d) = \frac{1}{\rho_s\sqrt{\pi}} \int \mathrm{d}x_s \exp\left(-\frac{x_s^2}{\rho_s^2}\right) \times \cos\left(\frac{\pi}{\lambda\tilde{r}_d}\left[x_d + x_s\frac{r_d}{r_s} - R_d\right]^2\right) \tag{32}$$

Here $R_d = Rr_t/r_s$ is the fiber radius projected to the detector, $\tilde{r}_d = r_d r_t/r_s$. The function $C(x_d)$ is calcu-

lated analytically. It is convenient to write the result as follows:

$$C(x_d) = \mathrm{Re}\left[\frac{1}{(1-i\beta)^{1/2}}\exp\left(i\frac{\pi(x_d-R_d)^2}{\lambda\tilde{r}_d(1-i\beta)}\right)\right] \tag{33}$$

where

$$\beta = \frac{\pi r_d \rho_s^2}{\lambda r_s r_t} \tag{34}$$

The parameter β depends on the source radius ρ_s. We take into account that $\beta \ll 1$ for the considered experimental conditions. Namely, when $\rho_s = 17$ μm, $r_s = 41$ m, $r_d = 5$ m, $\lambda = 0.073$ nm we have $\beta \approx 0.04$. Therefore we may neglect β as compared to unity in all terms except the cosine argument. As a result, we arrive at the following approximate expression:

$$C(x_d) = \cos\left(\pi\frac{(x_d-R_d)^2}{\lambda\tilde{r}_d(1+\beta^2)}+\frac{\beta}{2}\right)\times\exp\left(-\frac{(x_d-R_d)^2}{2s^2l_{tc}^2}\right) \tag{35}$$

where l_{tc} is the transverse coherence length at the object (see Eq. (12)) and $s = r_t/r_s$ is a scaling factor, so that sl_{tc} is the transverse coherence length projected to the detector.

To obtain the analytical expression for a visibility $V(x_d)$ we substitute Eqs. (31) and (35) in Eq. (1)

$$V(x_d) = V_0(x_d)\exp\left(-\frac{(x_d-R_d)^2}{2s^2l_{tc}^2}\right),$$
$$V_0(x_d) = \frac{2A(x_d)}{1+A^2(x_d)} \tag{36}$$

Here $V_0(x_d)$ is a visibility corresponding to the point source. The function $A(x_d)$ is defined by Eq. (30) where the following approximation for $f(x_d)$ may be used:

$$f(x_d) = \frac{(2\delta r_d)^2 R_d}{(x_d-R_d)^3} \tag{37}$$

The visibility $V(x_d)$ can be measured from experimental data for the intensity beat located at any point. If all the parameters of the experiment such as λ, δ, R, r_s and r_d are known then the function $V(x_d)$ contains only one unknown parameter, namely, the source size w_s. In principle each fringe can be used for the estimation of the source size when the damping of the visibility follows to the law (36). We write the formula that shows the source size in an explicit form

$$w_s = \frac{2\lambda r_t}{\pi(x_d-R_d)}\ln^{1/2}\left(\frac{V_0(x_d)}{V(x_d)}\right) \tag{38}$$

through the measured visibility V of the fringes and calculated theoretical visibility V_0 for the point source.

Let us discuss another possibility. It follows from Eq. (38) that the source size projection $w_s r_d/ r_s$ becomes comparable with the distance between the fringes $d_f = \lambda s r_d (x_d - R_d)^{-1}$ when $V(x_d) \approx V_0(x_d)\exp(-\pi^2/4) \approx 0.04 V_0(x_d)$. For far fringes $V_0(x_d) \approx f^{1/2}(x_d)$. Thus the visibility of the fringes having the distance between them comparable to the source size projection may be estimated as $V \approx 0.08\delta(R_d/r_d)^{1/2}(d_f/\lambda)^{3/2}$. Therefore one may find the fringes having the distance d_f between them and the visibility V which satisfy the condition $Vd_f^{-3/2} \approx 0.08\delta(R_d/r_d)^{1/2}\lambda^{-3/2}$ and then estimate the source size as $w_s \approx d_f r_s/r_d$. Substituting the parameters of the experiment we obtain that such fringes have the visibility $V \approx 0.007$. It is rather small value.

Since one should be careful in determining the distance between fringes of small visibility, it is more accurate to use the formula (38). Just this formula was used for the estimation of the ESRF source size (see above). To verify the estimation Fig. 6(a) shows the accurate theoretical intensity distribution at the detector for the parameters of experiment in the case of point source as a square modulus of Eq. (20). The calculation was performed for the real sample, namely, the boron fiber having a tungsten core (see Section 2). One may see the tungsten core influence the fringes in the region outside the fiber shadow. However, the main feature is that the damping of the fringes is not fast. Fig. 6(b) shows averaged over the source size 33 μm intensity distribution according to Eq. (8). Now the calculated intensity profile reproduces the experimentally measured one (Fig. 2). The contrast and the distance between the fringes

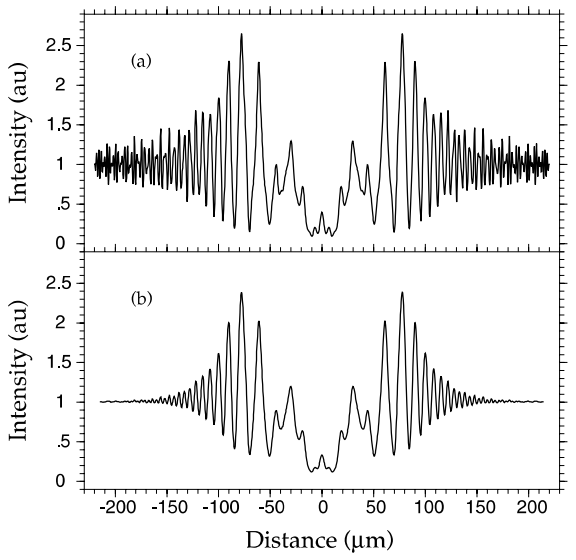

Fig. 6. The computer simulations of the 100 μm diameter fiber image with a point source (a) and a real source of 33 μm size (b).

coincide very closely. However, the experimental pattern contains some extra perturbations of the fringes caused by imperfections of the optical elements in the beam path, in particular vacuum windows, filters and monochromator crystals. There is also a problem to fit the central part of the fiber image. The reason may be that the size of the tungsten core is not known accurately.

5. Analytical theory of the slit image

5.1. Exact formula

Our experimental results show well resolved fringes on the diffraction pattern of slits of different sizes. Similar to the fiber case (see Section 4) in order to measure the source size from the visibility of the fringes we need the analytical theory for a quantitative usage of this technique. It is evident that in the case of slit the fringes have a diffraction origin. The fringes of apparent visibility arise in the Fresnel region of diffraction where the slit size a is comparable with the radius of the first Fresnel zone $\sqrt{\lambda r_d}$, where λ is a wavelength and r_d is the slit-to-detector distance. The distance satisfying this condition $r_d = a^2/\lambda$ is known as a Rayleigh distance.

Let us consider a simple optical setup where the point radiator on the source having a transverse coordinate $x_s = 0$ creates spherical monochromatized wave inside the slit located at the distance r_s. The slit restricts the wave front in accord to the relation $|x| < a/2$. We are interested in the transverse wavefield distribution at the distance r_d from the slit where the detector is placed.

Substituting Eq. (5) to Eq. (6) we obtain the integral

$$\frac{E(x_d)}{E_S(x_d)} = \frac{1}{\sqrt{i\lambda r_r}} \int_{-a/2}^{a/2} dx \exp\left(i \frac{\pi}{\lambda r_r} \left[x - x_d \frac{r_s}{r_t} \right]^2 \right) \tag{39}$$

which can be expressed as a sum of two complex normalized Fresnel integrals (see Eq. (29)) as follows:

$$\frac{E(x_d)}{E_S(x_d)} = [F(\gamma(1+\alpha)) + F(\gamma(1-\alpha))] \tag{40}$$

where $\alpha = 2x_d/a_d$ is a dimensionless coordinate at the detector, $a_d = ar_t/r_s$ is the slit width projected to the detector, $\gamma = a(2\lambda r_r)^{-1/2}$.

The complex Fresnel integral $F(x)$ has a well known asymptotic series expansion (see, for example, Ref. [40])

$$\lim_{x\to\infty} F(x) = \frac{1}{2} + \frac{\exp(i\pi x^2/2)}{i\pi x\sqrt{2i}} \times \left(1 + \frac{1}{i\pi x^2} + \frac{1\cdot 3}{(i\pi x^2)^2} + \cdots \right) \tag{41}$$

Different approximate expressions of the Fresnel integral may be found in the literature (see, for example, Ref. [40]). For a computer simulations the formulas of larger accuracy were used which are proposed, in a NAG library of Fortran procedures.

5.2. Asymptotic intensity at the center of slit image

We want to derive the approximate analytical expression for the basic parameters of the fringes using the asymptotic series expansion (41). In the

central part of the diffraction pattern when $|\alpha| \ll 1$ we neglect α as compared to unity in all terms except arguments of cosine function. As a result, the normalized intensity distribution looks as follows:

$$I_0(x_d) \approx 1 + \frac{1}{(\pi\gamma)^2} + \frac{1}{(\pi\gamma)^2}\cos\left(2\pi\gamma^2\alpha\right) + \frac{2\sqrt{2}}{\pi\gamma}\cos\left(\frac{\pi}{2}\gamma^2\left[1+\alpha^2\right] - \frac{3\pi}{4}\right)\cos\left(\pi\gamma^2\alpha\right) \tag{42}$$

where only the first two terms of the expansion (41) were taken into account.

Let us consider the parameters of the experiment: $r_s = 31$ m, $r_d = 10$ m, energy of X-rays 18 keV and two slit sizes $a = 500$ μm (case 1) and 100 μm (case 2). Under these conditions the parameter γ equals 15.5 (case 1) and 3.1 (case 2) the values which may be considered as large and intermediate. As follows from Eq. (42) the structure of fringes in the case of large value of γ is rather complicated. The interference term is only essential, namely, the last term in Eq. (42). The central fringes are of rather small contrast, and these have uneven structure.

The basic sinusoidal oscillations having rather small period $p_b = a_d/\gamma^2 = 2.8$ μm are modulated by uneven extra structure having a variable period $p_a(n) = (a_d/\gamma)(\sqrt{n} - \sqrt{n-1})$ where n counts the fringes from the center of image. For example, $p_a(n) = 42.7,\ 17.7,\ 13.6$ μm for $n = 1, 2, 3$. With increasing the distance from the center of the slit image the period of long oscillations becomes comparable with the period of short oscillations and the fringes do not show some simple structure. In such a region the last term of Eq. (42) can be rewritten in more suitable form

$$I_{\text{int}}(x_d) = \frac{\sqrt{2}}{\pi\gamma}\left[\cos\left(\pi\gamma^2\left[\alpha\left(1-\frac{\alpha}{2}\right) - \frac{3}{4}\right] + \frac{\pi}{4}\right) + \cos\left(\pi\gamma^2\left[\alpha\left(1+\frac{\alpha}{2}\right) + \frac{3}{4}\right] - \frac{\pi}{4}\right)\right] \tag{43}$$

One can see that when $|\alpha|$ is not very small the period of one set of fringes becomes larger with increasing $|x_d|$ whereas the period of another set of fringes decreases. For larger value of $|x_d|$ we need to take into account the difference in weights of these two cosine functions. Namely, in the more accurate expression the weight of cosine having a longer period is an increasing function of $|x_d|$. The other cosine has the decreasing weight.

In the case 2, when γ is of order 3, we may still use approximately Eq. (42). However, the structure of diffraction fringes is turned out to be quite different. The sinusoidal oscillations have rather large period $p_b = a_d/\gamma^2 = 13.8$ μm. Therefore such oscillations are well suitable for the source size measurement. Due to the fact that the first period of the extra structure is rather long, the image of narrow slit does not show the extra structure. We may neglect the extra structure at least for the central intensity peak. Keeping in mind this case we accept the following expression for the intensity distribution in the central part of the diffraction pattern

$$I_0(x_d) \approx 1 + \frac{2\sqrt{2}}{\pi\gamma}\cos\left(\frac{\pi}{2}\gamma^2 - \frac{3\pi}{4}\right)\cos\left(2\pi\gamma^2\frac{x_d}{a_d}\right) \tag{44}$$

Roughly speaking, this approximation is valid only for the central intensity peak when the slit image contains few fringes only. However, this case is well reachable in experiments.

5.3. Visibility and a source size measurement

The integral of Eq. (8) with $I_0(x_d)$ given by Eq. (44) is calculated analytically and the result looks as follows:

$$I(x_d) = 1 + \frac{2\sqrt{2}}{\pi\gamma}\cos\left(\frac{\pi}{2}\gamma^2 - \frac{3\pi}{4}\right) \times \exp\left(-\frac{\rho^2}{2l_{tc}^2}\right)\cos\left(2\pi\gamma^2\frac{x_d}{a_d}\right) \tag{45}$$

where $\rho = a/2$. This formula means that the width of the central intensity oscillation is not changed by source size, whereas the amplitude depends apparently on the source size making it to be less pronounced. Therefore the visibility of the central fringe may be written as follows taking into account the explicit expression for the parameter γ:

$$V = V_0 \exp\left(-\frac{\rho^2}{2l_{tc}^2}\right),$$
$$V_0 = \frac{4a_0}{\pi a}\left|\cos\left(\pi\left[\frac{a^2}{a_0^2}-\frac{3}{4}\right]\right)\right| \quad (46)$$

where $a_0 = 2(\lambda r_d r_s/r_t)^{1/2}$. We note once again that this formula is valid when $a > a_0$. The parameter V is measured from the experimental data. If all the parameters of the experiment such as λ, a, r_s and r_d are known then the expression for V contains only one unknown parameter, namely, the source size w_s.

The formula for the source size w_s in explicit form looks as follows:

$$w_s = \frac{4\lambda r_s}{\pi a}\ln^{1/2}\left[\frac{V_0}{V}\right] \quad (47)$$

The specific feature of this technique is that the visibility of the central fringe for a point source depends strongly on the parameters of experiment and can disappear under definite conditions. Therefore for the estimation of the source size one need to take the data corresponding the maximum visibility of the central fringe to obtain the maximum accuracy.

Eqs. (46) and (47) were used for the estimation the ESRF ID22 undulator source size (see Section 2). Fig. 7(a) shows the theoretical intensity distribution for a point source. The intensity beats have a fine structure due to the properties of the Fresnel integrals, namely, Fresnel zones of high orders. The main peaks show a contrast of rather high level. Fig. 7(b) shows the interference pattern in the case of extended source of 35 μm size. Now the visibility of the central fringe in the calculated and measured interference patterns coincide. However the edge fringes and the slope of intensity outside the slit image are different. This is probably due to the fact that it was impossible to eliminate some extra modifications of the beam or uneven edges of the slit.

5.4. Edge diffraction

Let us discuss here the case of very large slit size when only the edge diffraction is observable. We will analyze the left edge diffraction when $x_d \approx -a_d$. It is convenient to introduce a new coordinate

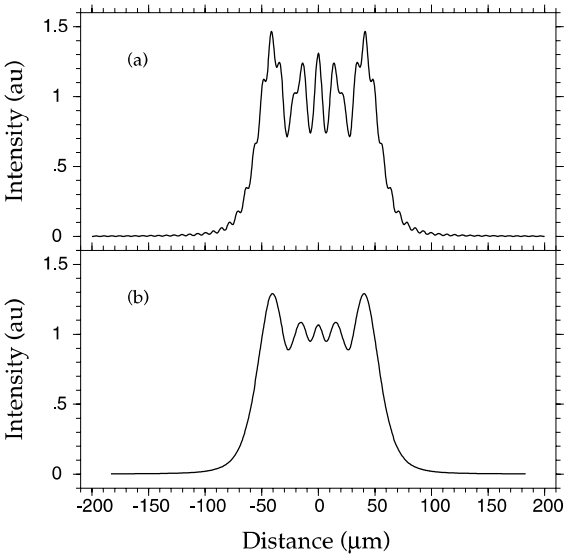

Fig. 7. The computer simulations of the 100 μm width slit image with a point source (a) and a real source of 35 μm size (b).

$u_d = x_d + a_d/2$ that is counted from the projection of the left edge of the slit to the detector and $|u_d| \ll a_d/2$. Negative u_d corresponds to a dark field (shadow of the screen), and positive u_d corresponds to a light field. Then using Eq. (40) one may write the normalized intensity for the point source as

$$I_0(u_d) = \left|\frac{1}{2} + F(bu_d)\right|^2, \quad b = \left(\frac{2r_s}{\lambda r_d r_t}\right)^{1/2} \quad (48)$$

Fig. 8 shows the intensity distribution calculated for the same parameters as for fiber image, namely, 17 keV X-rays, $r_s = 41$ m, $r_d = 5$ m. The intensity oscillations near the unit background in the light field have a rather simple sinusoidal structure of decreasing the amplitude and the period. The far fringes having an index $n > 4$ may be described analytically within the asymptotic approximation of Fresnel integral (see Eq. (41))

$$I_0(u_d) \approx 1 + \frac{1}{2\pi^2 b^2 u_d^2} + \frac{\sqrt{2}}{\pi b u_d}\cos\left(\frac{\pi}{2}\left[b^2 u_d^2 - \frac{3}{2}\right]\right) \quad (49)$$

Once again to obtain the real intensity distribution detected by detector we need to apply Eq. (8). When $bu_d > 4$ the second term is negligible. If

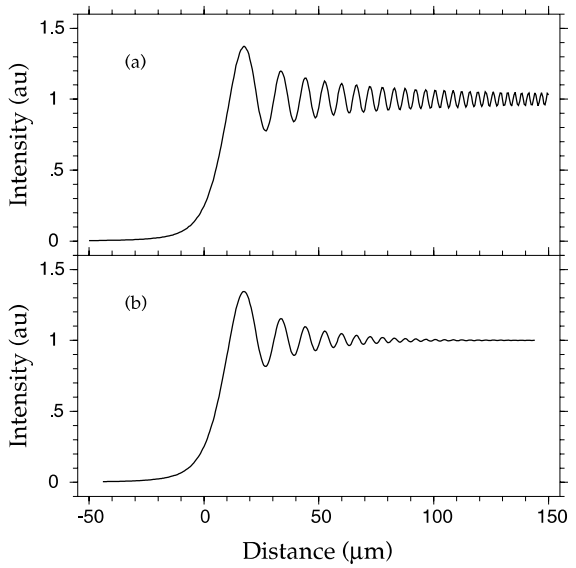

Fig. 8. The computer simulations of the wide slit edge image with a point source (a) and a real source of 33 μm size (b).

the source size projection is less than $1/b$ then we may average only the cosine function. As a result, the fringes pattern is described by

$$I(u_d) \approx 1 + \frac{\sqrt{2}}{\pi b u_d} C(u_d), \quad b u_d > 4 \tag{50}$$

where the integral $C(u_d)$ is similar to that considered in Section 4 (see Eq. (32))

$$\begin{aligned} C(u_d) &= \frac{1}{\rho_s \sqrt{\pi}} \int dx_s \exp\left(-\frac{x_s^2}{\rho_s^2}\right) \\ &\quad \times \cos\left(\frac{\pi}{2} b^2 \left[u_d + x_s \frac{r_d}{r_s}\right]^2 - \frac{3\pi}{4}\right) \\ &= \mathrm{Re}\left[\frac{1}{(1-i\beta)^{1/2}} \exp\left(i\frac{\pi b^2 u_d^2}{2(1-i\beta)} - i\frac{3\pi}{4}\right)\right] \\ &= \cos\left(\frac{\pi b^2 u_d^2}{2(1+\beta^2)} + \frac{\beta}{2} - \frac{3\pi}{4}\right) \exp\left(-\frac{u_d^2}{2 s^2 l_{tc}^2}\right) \end{aligned} \tag{51}$$

Here β is defined by Eq. (34) and we made the same assumptions as in the fiber section. The visibility is equal to

$$\begin{aligned} V(u_d) &= V_0(u_d) \exp\left(-\frac{u_d^2}{2 s^2 l_{tc}^2}\right), \\ V_0(u_d) &= \frac{\sqrt{\lambda r_d r_t / r_s}}{\pi u_d} \end{aligned} \tag{52}$$

As before, the source size is determined by

$$w_s = \frac{2 r_t}{\pi u_d} \ln^{1/2}\left(\frac{V_0(u_d)}{V(u_d)}\right) \tag{53}$$

For a practical implementation of this technique one needs to measure accurately the coordinate u_d on the edge image. One may use for this purpose the accurate value of the normalized intensity at $u_d = 0$. To obtain this we note that in the region of small $|u_d|$ in the case of the point source the intensity is described by

$$\begin{aligned} I_0(u_d) &\approx \frac{1}{4} + \frac{x}{2} + \frac{x^2}{2} + \frac{\pi x^3}{12} - \frac{\pi^2 x^5}{40} - \frac{13\pi^2 x^6}{360} + \cdots, \\ x &= b u_d \end{aligned} \tag{54}$$

The intensity for the real source $I(0)$ is obtained applying Eq. (8). It is evident that the odd terms give zero contributions. The integrals are calculated analytically and we arrive to the estimation

$$I(0) \approx \frac{1}{4} + \frac{C_2}{2} a_s - \frac{13\pi^2 C_6}{360} a_s^3 + \cdots \tag{55}$$

where

$$\begin{aligned} a_s &= \frac{w_s^2 r_d}{2\lambda r_s r_t}, \\ C_n &= \frac{1}{\sqrt{\pi}} \int dt\, t^n \exp(-t^2) = \frac{(n-1)}{2} C_{n-2} \end{aligned} \tag{56}$$

The coefficients $C_2 = 1/2$ and $C_6 = 15/8$ are found from the recurrent relation and $C_0 = 1$. It is easy to evaluate the parameter a_s as 0.07 in the case: 18 keV X-rays, $r_s = 31$ m, $r_d = 10$ m, $w_s = 35$ μm. Hence the value 1/4 of the normalized intensity may be used with a good accuracy to find the zero point on the edge image.

6. Conclusion

The method of direct measuring the source size and the transverse coherence length is proposed and tested at the undulator beamline ID22 at the

ESRF (Grenoble). The simple in-line holographic setup was used to detect the diffraction patterns (phase contrast images) of high quality for the well calibrated microobjects like the boron fiber of about 100 μm diameter or the slit of about 100 μm width or the edge of the wide slit. The real fringe pattern is compared with ideal one simulated theoretically for the point source. The analytical theory of both the fiber diffraction image and the slit diffraction image is developed and simple formulas were derived for the source size and the transverse coherence length. These formulas allows us to estimate the source size as (35 ± 4) μm, which is in accordance with the data provided by ESRF machine group at the time of experiment. The analytical results were confirmed by accurate computer simulations. The proposed technique is well suited for the third-generation synchrotron sources. The advantages of this technique are the simplicity and high accuracy due to the absence of optical elements that may deteriorate the quality of the X-ray beam. On the other hand, this technique allows one to characterize the coherence preservation by optical elements installed in the setup. In view of future X-ray free electron laser development this technique is promising and is of particular interest.

References

[1] A. Snigirev, I. Snigireva, V. Kohn, S. Kuznetsov, I. Schelokov, Rev. Sci. Instrum. 66 (1995) 5486–5492.

[2] C. Raven, A. Snigirev, I. Snigireva, P. Spanne, A. Souvorov, V. Kohn, Appl. Phys. Lett. 69 (1996) 1826–1828.

[3] Z.H. Hu, P.A. Thomas, A. Snigirev, I. Snigireva, A. Souvorov, P.G.R. Smith, G.W. Ross, S. Teat, Nature 392 (1998) 690–693.

[4] P. Cloetens, R. Barrett, J. Baruchel, J.P. Guigay, M. Schlenker, J. Phys. D: Appl. Phys. 29 (1996) 133–146.

[5] K.A. Nugent, T.E. Gureyev, D.F. Cookson, D. Paganin, Z. Barnea, Phys. Rev. Lett. 77 (1996) 2961–2964.

[6] C. Raven, A. Snigirev, A. Koch, I. Snigireva, V. Kohn, SPIE 3149 (1997) 140–148.

[7] V.G. Kohn, Physica Scripta 56 (1997) 14–19.

[8] P. Spanne, C. Raven, I. Snigireva, A. Snigirev, Phys. Med. Biol. 44 (1999) 741–749.

[9] T.E. Gureyev, C. Raven, A. Snigirev, I. Snigireva, S.W. Wilkins, J. Phys. D: Appl. Phys. 32 (1999) 563–567.

[10] G. Margaritondo, G. Tromba, J. Appl. Phys. 85 (1999) 3406–3408.

[11] P. Cloetens, W. Ludwig, J. Baruchel, D. Van Dyck, J. Van Landuyt, J.P. Guigay, M. Schlenker, Appl. Phys. Lett. 75 (1999) 2912–2914.

[12] A. Koch, C. Raven, P. Spanne, A. Snigirev, J. Opt. Soc. Am. 15 (1998) 1940–1951.

[13] A. Snigirev, Rev. Sci. Instrum. 66 (1995) 2053–2058.

[14] I. Snigireva, A. Souvorov, A. Snigirev, in: J. Thieme, G. Schmahl, D. Rudolph, E. Umbach (Eds.), X-ray Microscopy and Spectroscopy, Springer, Berlin, 1998, pp. IV37–IV44.

[15] W. Yun, B. Lai, Z. Cai, J. Masser, D. Legnini, E. Gluskin, Z. Chen, A. Krasnoperova, Y. Vladimirsky, F. Cerrina, E. Di Fabrizio, M. Gentili, Rev. Sci. Instrum. 70 (1999) 2238–2241.

[16] W. Yun, B. Lai, A.A. Krasnoperova, E. De Fabrizio, Z. Cai, F. Zerrina, Z. Chen, M. Gentilli, E. Gluskin, Rev. Sci. Instrum. 70 (1999) 3537–3541.

[17] A. Snigirev, V. Kohn, I. Snigireva, B. Lengeler, Nature 384 (1996) 49–51.

[18] B. Lengeler, C. Schroer, M. Richwin, J. Tummler, M. Drakopoulos, A. Snigirev, I. Snigireva, Appl. Phys. Lett. 74 (1999) 3924–3926.

[19] Y. Takayama, R.Z. Tai, T. Hatano, T. Miyahara, W. Okamoto, Y. Kagoshima, J. Synchrotron Rad. 5 (1998) 456–458.

[20] Y. Takayama, T. Hatano, T. Miyahara, W. Okamoto, J. Synchrotron Rad. 5 (1998) 1187–1194.

[21] J.E. Trebes, K.A. Nugent, S. Mrowka, R.A. London, T.W. Barbee, M.R. Carter, J.A. Koch, B.J. MacGowan, D.L. Matthews, L.B. Da Silva, G.F. Stone, M.D. Feit, Phys. Rev. Lett. 68 (1992) 588–591.

[22] T. Ishikawa, Acta Crystallogr. A 44 (1988) 496–499.

[23] K. Fezzaa, F. Comin, S. Marchesini, R. Coisson, M. Belakhovsky, J. X-ray Sci. Technol. 7 (1997) 12–23.

[24] A. Snigirev, SPIE 2856 (1996) 26–33.

[25] I. Schelokov, O. Hignette, C. Raven, A. Snigirev, I. Snigireva, A. Souvorov, SPIE 2805 (1996) 282–292.

[26] A. Souvorov, I. Snigireva, A. Snigirev, SPIE 3113 (1997) 476–483.

[27] A. Souvorov, M. Drakopoulos, I. Snigireva, A. Snigirev, J. Phys. D: Appl. Phys. 32 (1999) A184–A192.

[28] A. Snigirev, I. Snigireva, V. Kohn, S. Kuznetsov, Nucl. Instrum. Meth. A 370 (1996) 634–640.

[29] P. Cloetens, J.P. Guigay, C. De Martino, J. Baruchel, M. Schlenker, Opt. Lett. 22 (1997) 1059–1061.

[30] V. Kohn, I. Snigireva, A. Snigirev, Phys. Rev. Lett. 85 (2000) 2745–2748.

[31] A.V. Baez, H.M.A. El-Sum, in: V.E. Cosslett, A. Engström, H.H. Pattee (Eds.), X-ray Microscopy and Microradiography, Academic Press, New York, 1957, pp. 347–366.

[32] G.A. Tyler, B.J. Thompson, Optica Acta 23 (1976) 685–700.

[33] M. Born, E. Wolf, Principles of Optics, Pergamon Press, Oxford, 1986.

[34] E. Hecht, Optics, Addison-Wesley, Reading, MA, 1998.
[35] A.M. Afanas'ev, V.G. Kohn, Sov. Phys. Crystallogr. 22 (1977) 355.
[36] J. Cowley, Diffraction Physics, North-Holland, Amsterdam, 1981.
[37] R.W. James, The Principles of the Diffraction of X-rays, Cornell University Press, Ithaca, NY, 1967.
[38] S.K. Sinha, M. Tolan, A. Gibaud, Phys. Rev. B 57 (1998) 2740–2758.
[39] H. Jeffreys, B. Swirles, Method of Mathematical Physics, Cambridge University Press, Cambridge, 1966.
[40] M. Abramowitz, I.A. Stegun (Eds.), Handbook of Mathematical Functions, Applied Mathematic Series, vol. 55, National Bureau of Standards, Washington, 1964.